

PCCP

Accepted Manuscript



This is an *Accepted Manuscript*, which has been through the Royal Society of Chemistry peer review process and has been accepted for publication.

Accepted Manuscripts are published online shortly after acceptance, before technical editing, formatting and proof reading. Using this free service, authors can make their results available to the community, in citable form, before we publish the edited article. We will replace this *Accepted Manuscript* with the edited and formatted *Advance Article* as soon as it is available.

You can find more information about *Accepted Manuscripts* in the [Information for Authors](#).

Please note that technical editing may introduce minor changes to the text and/or graphics, which may alter content. The journal's standard [Terms & Conditions](#) and the [Ethical guidelines](#) still apply. In no event shall the Royal Society of Chemistry be held responsible for any errors or omissions in this *Accepted Manuscript* or any consequences arising from the use of any information it contains.

ARTICLE

Combinatorial solar cell libraries for the investigation of different metal back contacts for TiO₂ / Cu₂O hetero-junction solar cells

Cite this: DOI: 10.1039/x0xx00000x

Received 00th January 2012,
Accepted 00th January 2012

DOI: 10.1039/x0xx00000x

www.rsc.org/

S. Rühle,^{a,*} H.-N. Barad,^{a,*} Y. Bouhadana,^a D. A. Keller,^a A. Ginsburg,^a
K. Shimanovich,^a K. Majhi,^a R. Lovrincic,^b A. Y. Anderson,^a and A. Zaban^a

Here we present a comprehensive investigation of TiO₂ / Cu₂O hetero-junction solar cells with different back contacts (Au, ITO, Cu or Ag). Combinatorial hetero-junction libraries, consisting of a linear TiO₂ thickness gradient produced by spray pyrolysis and a bell shaped Cu₂O profile synthesized by pulsed laser deposition were chosen to investigate the impact of the two metal oxide layer thicknesses. The back contacts were deposited as round patches onto a grid of 13 x 13 points, 169 contacts for each contact material, forming a library containing 4 x 13 x 13 = 676 back contacts. Each back contact represented a solar cell with an individual TiO₂ and Cu₂O thickness. I-V measurements show that all four materials provide an ohmic contact, and that the open circuit voltage of ~300 mV is rather independent of both layer thicknesses and contact material. The size of the Cu₂O crystals strongly decreases with distance from the center of deposition, which leads to a drastic increase of series resistance when the crystal size is <50nm.

Introduction

The market for photovoltaic (PV) modules has shown exponential growth over the last years yet in most places PV generated electricity still relies on subsidies.^{1, 2} To reach grid parity, further price reductions are required, which might be reached by up-scaling of existing production processes. However, larger price reductions could be reached with new PV materials that, ideally, should be cheap, not hazardous, and easy to manufacture using low cost fabrication methods.

Metal oxide (MO) semiconductors are promising candidates for photovoltaic applications; many MOs are abundant, non-toxic, and chemically stable, which enables material deposition under ambient conditions.³ Today, MOs are already widely used as components in commercially available solar cells as transparent conducting front electrodes, or as window layers, which improve the selectivity for electron collection at the front contact. In PV technologies based on nano-composite materials such as dye-sensitized solar cells,⁴ perovskite-sensitized solar cells,⁵⁻⁷ quantum-dot-sensitized solar cells,⁸⁻¹⁰ and extreme thin absorber solar cells,¹¹ MO nano-structures are used to provide a very high microscopic surface area for a thin absorber layer.

All-oxide photovoltaic hetero-junction cells are presently attracting significant attention, with ZnO/Cu₂O being the most investigated system.¹²⁻¹⁷ The wide band gap ZnO window layer acts as an electron transport layer, while the Cu₂O is the light absorber with a band gap at around 2eV.¹⁸ Remarkable

photovoltages of 690 mV with light to electric power conversion efficiencies up to 3.8% have been reported recently for ZnO/Cu₂O hetero-junction cells.¹⁴ With an alternative window layer such as Ga₂O₃ higher photovoltages up to 800 mV, and a light to electric power conversion efficiency of 5.4% were achieved.¹⁹ This is calling for the investigation of novel MOs and MO hetero-junctions, to further progress in the field of all-oxide photovoltaics.^{20, 21}

Combinatorial material science is a powerful tool for rapid screening of new material compositions^{22, 23} for a wide range of applications such as catalysis,²⁴ passivation,²⁵ solid state electrolytes²⁶ or solar water splitting.²⁷ In organic photovoltaics combinatorial methods have been used for the development of fullerene blends.²⁸ Here we apply the concept of combinatorial material science to the field of all-oxide photovoltaics.²⁹ In contrast to ZnO/Cu₂O hetero-junctions TiO₂/Cu₂O solar cells are much less investigated.^{20, 30} We present combinatorial TiO₂/Cu₂O hetero-junction device libraries for a comprehensive investigation how the thickness of both MO layers affects the solar cell performance using Au, ITO, Cu, and Ag as four different back contact materials. The implementation of combinatorial material science for photovoltaics allows understanding from a single device library the importance of crystal size, the inherent voltage limitation of a specific hetero-junction and the role of the back contact.

Experimental

Spray Pyrolysis of TiO₂: Commercially available Fluorine doped SnO₂ (FTO) coated glass substrates with a size of 71.2 x 71.2 mm², and a sheet resistance of 15 Ω/square (TEC 15, Hartford Glass Co. Inc.) were thoroughly washed with soap, rinsed with ethanol followed by de-ionized water, and were dried under a dry air stream. Compact TiO₂ layers were deposited by spray pyrolysis, where the substrates were placed onto a Ceran hotplate (Harry Gestigkeit GmbH). A precursor solution of 0.1 M Titaniumtetraisopropoxide and 0.1 M Acetylacetone in Ethanol and Isopropanol (mixing ratio 1:1) was sprayed with a pneumatic spray nozzle (Spraying Systems Co.) onto the substrates at a hotplate temperature of 450 °C. The nozzle was mounted onto a commercial x-y-z scanner (EAS GmbH),^{31, 32} the precursor flow rate of 60 cm³/hr was controlled by a syringe pump (Razel Scientific Instruments), while clean dehumidified compressed air, at a flow rate of 6 l/min, was used as a carrier gas. The x-y scan velocity was 30 mm/s, and the nozzle to substrate distance was approximately 6.9 cm. For combinatorial device fabrication a linear thickness gradient was produced using a series of spray cycles with a successively decreasing scan area.

Pulsed Laser Deposition of Cu₂O: The Cu₂O absorber was deposited by pulsed laser deposition (PLD) using a commercial system (Neocera) consisting of a KrF excimer laser with an emission wavelength at 248 nm (Coherent, CompexPro102). The square substrates were placed into the PLD system in front of the radiative heating stage using a custom made sample holder. Deposition was carried out at a target to sample distance of 67 mm, a heater temperature of 400 °C, and an Ar pressure of 150 mTorr. A laser fluence inside the vacuum chamber of 70 mJ, and a laser spot size of 7.2 mm², were measured, corresponding to an energy density of ~1 J/cm². Deposition was carried out using a Cu₂O target with a purity of 99.9% (Kurt J. Lesker Co.). To achieve the inhomogeneous thickness profile required for combinatorial device libraries, the target was ablated by 60,000 laser pulses at a repetition rate of 5 Hz without sample rotation.

Deposition of Electrical Contacts: For *I-V* characterization the FTO substrate served as a transparent conducting front electrode. To provide a good electrical contact to the measurement system, the TiO₂ and Cu₂O layer were mechanically removed close to the library edges using a diamond pen, followed by ultrasonic soldering (MBR Electronics) of a thin frame of a soldering alloy around the device library.

As back contacts, a grid of 13 x 13 metal patches was deposited either by sputtering or by thermal evaporation onto the Cu₂O layer using a shadow mask. Each contact patch had a diameter of 1.8 mm, corresponding to an area of ~0.026 cm², which defined the solar cell area. Rotating the shadow mask by 90°, 180° and 270° provided a way to deposit four different back contact materials, each of which on a grid of 13 x 13 contacts points (see Fig. 1). In this work Au, Ag, ITO, and Cu contact patches were investigated, and their thicknesses were ~100 nm. Au, ITO, and Cu were deposited by sputtering while Ag was thermally evaporated. To provide for each contact material a good electrical connection to the measurement system, the ITO and Cu patches were additionally covered with a 40 nm thick layer of Au.

Structural Characterization: Structural characterization of the PV cell library was carried out before deposition of the metal back contacts. X-ray diffraction measurements were performed with a Rigaku Smartlab work station with a θ - 2θ scan range from 25° to 80° on 4 different points. SEM measurements were carried out in the same points using a Helios 600 system (FEI).

Optical Characterization: Optical transmission and reflectance spectra were measured with a homebuilt mapping system, consisting of a computer controlled x-y scanning table (Märzhäuser Wetzlar GmbH & Co. KG) in conjunction with a specular reflectance probe and two integrating spheres, connected by optical fibers to CCD array spectrometers (HR4000, Ocean Optics Inc.).³³ Total transmittance, total reflectance, and specular reflectance were measured after the deposition of each layer.

Thickness Analysis: The thickness of the TiO₂ layer was determined using commercial available optical modeling software (CODE),³⁴ fitting simulated reflection and transmission spectra, in a spectral range from 350 – 1000 nm, to the measured ones with the TiO₂ thickness, d_{TiO_2} , as a fit parameter. The simulation was based on the OJL interband transition model,³⁵ and it was validated on different samples using SEM images of focused ion beam (FIB) produced cross-sections.

The Cu₂O thickness, $d_{\text{Cu}_2\text{O}}$, was derived from total transmission (TT) and total reflectance (TR) data at 480 nm ($d_{\text{Cu}_2\text{O}} = \alpha(480\text{nm})^{-1} \log(\text{TT}(480\text{nm})/(1 - \text{TR}(480\text{nm})))$) using an absorption coefficient, $\alpha = 1.4 \cdot 10^5 \text{ cm}^{-1}$ at 480 nm (2.58 eV).³⁶ The Cu₂O thickness derived from optical measurements was verified by thickness determination from cross-section SEM measurements taken at the maximum thickness of the deposition profile, both measured and calculated thicknesses were in good agreement with each other.

Solar Cell Characterization The *I-V* characteristics of all 676 solar cells (169 for each contact type) were measured with a homebuilt automated scanning *I-V* system consisting of a Keithley 2400 source meter, an x-y scanning table (Märzhäuser Wetzlar GmbH & Co. KG) in conjunction with a motorized z-arm (Olympus/Märzhäuser Wetzlar GmbH & Co. KG) and a laser pumped Xe lamp (LDLS, from Energetics Co.), which was coupled through an optical fiber to the scanning stage. The solar cell device library was placed onto the x-y stage and mechanically clamped using metal clips, which also provided the electrical connection between the FTO via the soldered metal frame, and the source meter for electrical measurements (Keithley 2400). Temporary electrical contact to each individual solar cell was established by a gold plated spring loaded tip (Ingun Prüfmittelbau GmbH), mounted onto the motorized z-arm, touching the back contact metal patch for the duration of the measurement. After each measurement was completed the tip was lifted and the x-y scanning table moved the library to the next contact patch. For each point the *I-V* curve was measured twice, in ascending and descending scan direction, to exclude capacitive effects due to charge trapping. Solar cells which showed a difference of more than 15% in the open circuit voltage (V_{oc}), short circuit current (I_{sc}), or the fill factor were not considered for further analysis, as well as *I-V* curves that showed less than three measurement points in the quadrant of photovoltaic action.

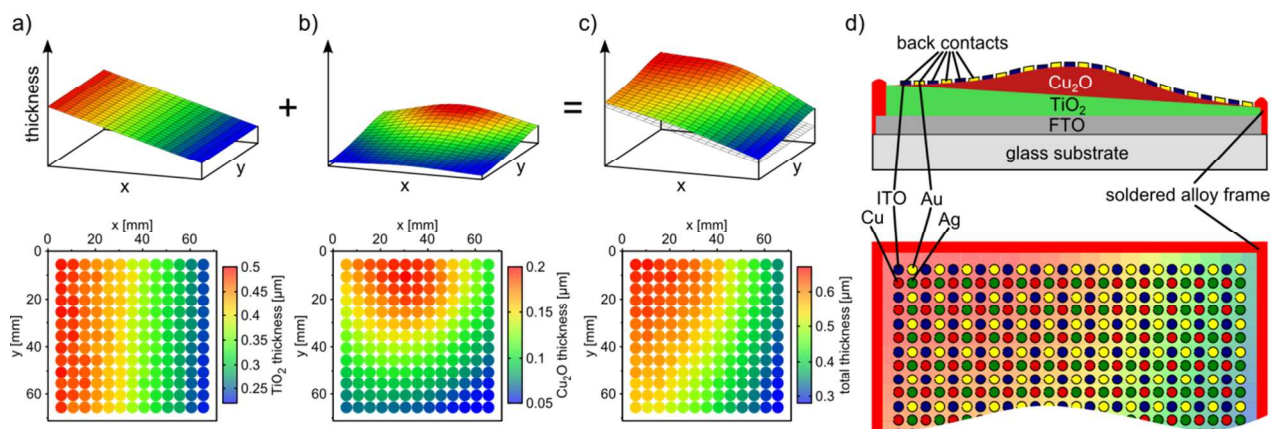


Figure 1. Combinatorial PV device library design. a) Synthesis of a compact TiO_2 layer with a linear thickness gradient along the x -axis, deposited onto a FTO covered glass substrate. The bottom shows a top view where different colors represent the varying thickness of the layer. b) Thickness profile described by eq. (1) of the Cu_2O absorber deposited by PLD. c) Joint thickness profile of the absorber deposited onto the linear TiO_2 gradient. d) Cross-section and top view of a combinatorial device library. The FTO layer serves as a joint front contact which is electrically connected via an ultrasonically soldered tin alloy frame (red). Four arrays of 13×13 round back contacts have been used to investigate different back contact materials. Each contact patch defines a single PV cell.

The light spectrum of the Xe lamp was adjusted to the sun spectrum using an AM1.5G filter. Furthermore, a long pass filter was used to suppress all photons with a wavelength shorter than 400 nm, in order to exclude the excitation of electron-hole pairs within the TiO_2 . The illumination was confined to a round spot with a diameter of ~ 6 mm using a collimating lens. The light intensity of 95.4 mW/cm^2 (corresponding to the AM1.5G spectrum without photons that have a wavelength below 400nm), was adjusted by neutral density filters and by varying the distance between the collimator lens and the device library.

Data Acquisition: Labview programming was used to control the scanning systems for optical and solar cell characterization, and for data acquisition. Solar cell parameters from the I-V curves were derived using a Matlab script while Gnuplot was used for graphical data representation.

Results and Discussion

A scheme of the combinatorial $\text{TiO}_2/\text{Cu}_2\text{O}$ hetero-junction solar cell library with four different grids of back contacts is shown in Figure 1. The thickness profile of the linear TiO_2 gradient is schematically shown in Fig. 1a (top) while the bottom shows TiO_2 thickness data derived from optical measurements ranging from 200 – 500 nm. The bell-shaped Cu_2O profile in Fig. 1b can be approximately described by^{37,38}:

$$d(x, y) = d_0 \cos^{n_x}(\alpha_x) \cos^{n_y}(\alpha_y) \quad (\text{eq. 1})$$

with $\alpha_x = \text{atan}((x - x_0)/h)$
and $\alpha_y = \text{atan}((y - y_0)/h)$,

using the substrate coordinates x and y and the maximum deposition thickness d_0 at the center of the plasma plume located at (x_0, y_0) . The distance between the FTO substrate and the Cu_2O target is denoted by h , and the exponents n_x and n_y

depend on PLD parameters such as pressure in the deposition chamber, laser power, and laser focus on the target.^{38, 39} Thickness data derived from optical measurements are shown at the bottom of Fig. 1b with a maximum thickness of 200 nm, located at the top edge of the library, slightly off-centered towards the left side. The sum of the TiO_2 and Cu_2O thickness profiles is shown in Fig. 1c.

Structural analysis was carried out by scanning electron microscopy (SEM) and X-ray diffraction (XRD). Figure 2 shows measurements taken at four different points of the hetero-junction library from the top at the highest Cu_2O thickness down to the bottom edge of the library, which has a Cu_2O thickness ~ 60 nm. The locations of the measured points are schematically shown by bold blue dots, superimposed onto the Cu_2O thickness profile map (inset of Fig. 2a). The morphology shown in the SEM images clearly reveals the cubic Cu_2O structure with the largest crystal size of ~ 150 nm near the deposition maximum, in the center of the deposition plume at the top of the library (Fig. 2a(i)). With increasing distance from the center of plume the crystal size decreases down to ~ 60 nm, at the bottom of the library (Fig. 2a(vi)). Droplets were observed in the vicinity of the center of plume while the major part of the library was droplet free.

XRD measurements show pronounced peaks of Cu_2O at 29.55° (110), 36.42° (111), 42.30° (200) and 61.36° (220) with a decreasing intensity at the bottom of the library where the Cu_2O thickness was around 70 nm. Furthermore, TiO_2 anatase peaks can be recognized at 25.28° (120), 37.80° (012), and 68.76° (116) as well as rutile peaks at 36.09° (131) and 39.19° (040). To find the rutile phase besides anatase in the spray pyrolysis deposited TiO_2 layer was unexpected due to a deposition temperature of 450°C , which is below the phase transition temperature from anatase to rutile. However, it is possible that the local temperature in the spray zone was higher due to the release of energy (heat) from the pyrolysis process, which might explain the existence of the rutile phase.

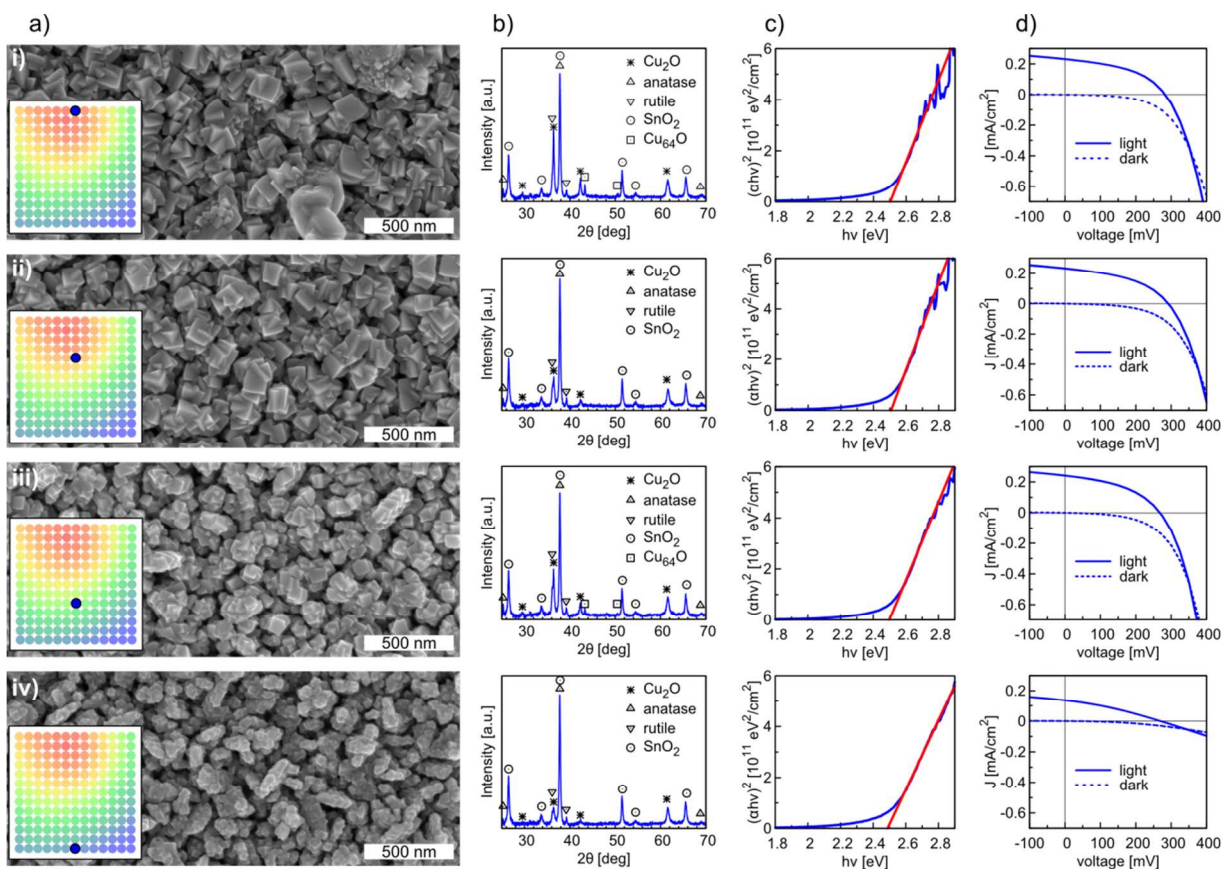


Figure 2. a) SEM images, b) XRD spectra, c) Tauc plots and d) I - V measurements taken at four different locations of the hetero-junction library shown in the insets of a) as blue points superimposed to the Cu_2O thickness profile: i) At the library top edge close to the center of the Cu_2O deposition, ii) 1/3 below the top edge, iii) 2/3 below the top edge and iv) at the bottom of the library. SEM, XRD and optical transmission and reflection measurements were performed before the deposition of the back contacts. The I - V curves (d) were measured using the Cu back contacts.

SnO_2 peaks at 26.51° (110), 33.77° (101), 37.84° (200), 51.61° (211), 54.59° (220) and 65.75° (301) which originate from the FTO layer are also seen. The relative peak intensities of the TiO_2 and SnO_2 remain constant from top to bottom of the library, due to the constant thickness of both layers in this direction of the library. Besides these peaks two rather weak peaks appear at 43.29° and 50.42° at the top (i) and in the lower half of the library (iii) of Fig. 2 that coincide with peaks of Cu_{64}O . This might be an indication for a copper rich phase, either at the $\text{TiO}_2/\text{Cu}_2\text{O}$ interface, in the Cu_2O bulk, or on the surface (note that XRD spectra were recorded before the deposition of the back contact). Copper rich phases are a well-known limitation for metal/ Cu_2O Schottky junction solar cells, because the formation of a Cu rich phase at the interface determines the Schottky barrier height, and thus limits the achievable photovoltage.⁴⁰ Also for metal oxide / Cu_2O hetero-junctions the existence of a copper rich phase has been discussed.⁴¹

Tauc plots⁴² of the hetero-junction library are shown in Fig. 2c, where the absorption coefficient α was derived from optical transmittance (TT) and reflectance spectra (TR), and the local Cu_2O thickness $d(x,y)$ according to

$$\alpha(\lambda) = -\frac{1}{d} \log \left(\frac{TT(\lambda)}{1-TR(\lambda)} \right) \quad (\text{eq. 2})$$

in a wavelength range from 350 – 1000 nm, corresponding to a photon energy of 1.24 – 3.54 eV. For direct band gap semiconductors the value of the band gap can be extracted from the intercept of a linear fit of $(\alpha h\nu)^2$ vs. $h\nu$ with the x -axis, shown as a red line in Fig. 2c. A band gap of 2.5 eV is derived in all four places of the library, which corresponds to the first symmetry allowed optical transition of Cu_2O .^{18, 36} The value of 2.5 eV is measured for the entire library, with a variation of ± 30 meV. Optical transitions at ~ 2 eV at room temperature, corresponding to the widely reported band gap of 2.18 eV at 4 K, are parity forbidden and thus very weak. Such transitions can in general be extracted from $(\alpha h\nu)^n$ vs. $h\nu$ plots with $n = 2/3$,⁴³ however with this $\text{TiO}_2 / \text{Cu}_2\text{O}$ library it was not possible to identify a clear linear regime suitable for fitting and extracting the symmetry forbidden transition.

After the deposition of four different back contact metals (Au, ITO, Cu and Ag), each of them deposited onto 13×13 grid points, I - V scans were performed using an automated measurement system with x - y scanning capability. A spring loaded Au coated metal tip was automatically brought to the metal patch making temporary electrical contact for each individual measurement while a metal clip provided permanent electrical contact *via* the soldered frame with the joint FTO

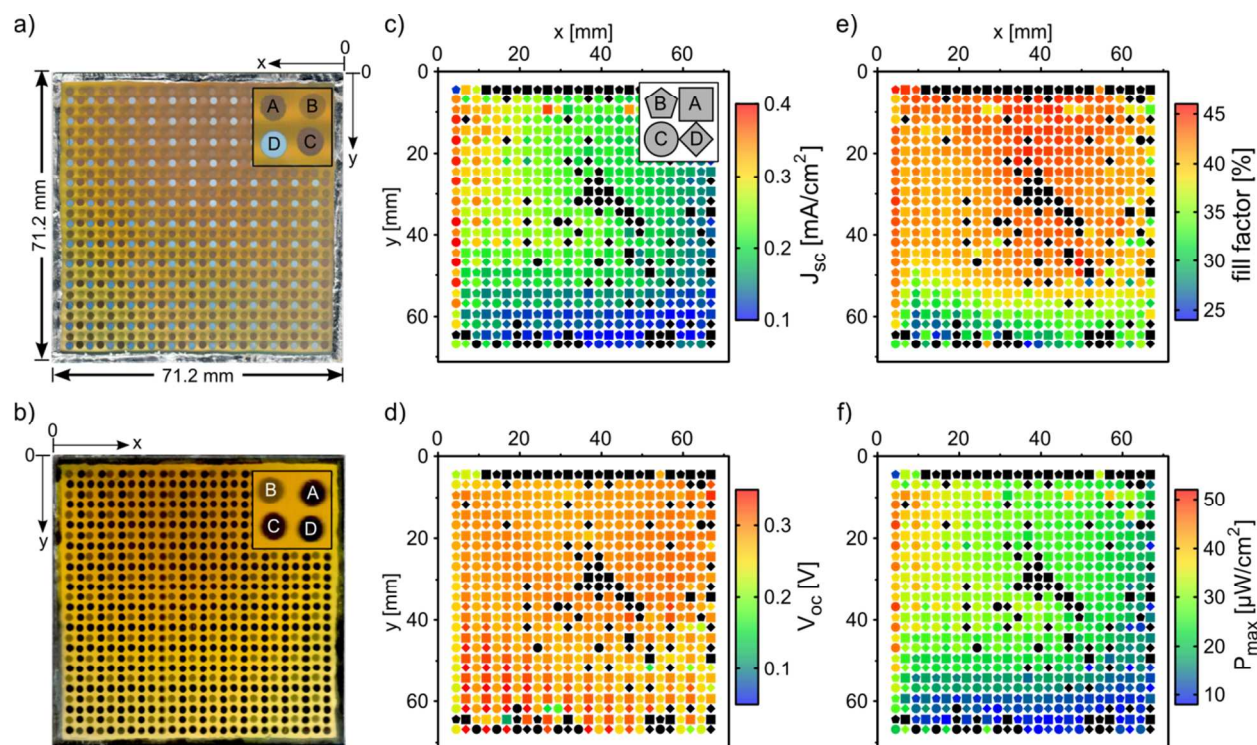


Figure 3. a) Photograph of the $\text{TiO}_2/\text{Cu}_2\text{O}$ hetero-junction library from the back contact side. The inset (top right) shows a magnification of four contacts with (A) Au, (B) ITO (C) Cu and (D) Ag. (B) and (C) were additionally covered with a 40nm thick Au layer for better electrical contact to the measurement tip. b) Photograph of the PV library from the glass side. c) Map of the J_{sc} . d) V_{oc} e) fill factor and f) P_{max} . Cells with Au contacts are shown as squares, ITO contacts as pentagons, Cu contacts as circles and Ag contacts as diamonds. Non-photovoltaic cells or cells which were touching each other (top row) are shown as black points.

front contact. I - V scans were recorded in the dark and under illumination, where a laser pumped Xe lamp in conjunction with an AM1.5G filter and a 400 nm long pass filter were used as the light source, providing a spectrum in good agreement with sunlight but without the photons below 400 nm. By removing these photons electron hole generation was restricted to the Cu_2O light absorber. The current and power were normalized with respect to the metal contact area of 0.026 cm^2 . The patch size was a compromise between lateral resolution of the photovoltaic device library and a systematic error that is introduced due to edge effects around the contact patch. Edge effects can, for example, occur due to lateral charge carrier diffusion into the contact patch, such that the active PV cell area is larger than the geometric patch size. Consequently, current densities recorded on a single library can be compared with each other but for comparison with literature values measurement errors due to the small cell size might exist.⁴⁴ Figure 2d shows light and dark I - V curves measured at four different points of the library from maximum Cu_2O thickness of $\sim 200 \text{ nm}$ down to $\sim 60 \text{ nm}$. The first three cells (from top to bottom, as marked in the inset of Fig 2a) show a comparable performance while the cell with the thinnest Cu_2O layer has a poor rectifying behavior due to a high series resistance.

A complete library analysis of the PV parameters, J_{sc} , V_{oc} , fill factor and P_{max} , is presented in Fig. 3. Photographs of the libraries from the back contact side and from the glass side, through which the cells were illuminated, are shown in Fig. 3a and b, respectively. Note that the coordinate system is chosen with the origin in the top left corner of the library when looking

through the illumination side. In this representation the linear TiO_2 gradient is parallel to the x -axis, with the maximum TiO_2 thickness at the left and the minimum at the right hand side. The Cu_2O profile has its maximum close to the middle of the top edge of the library. The different contact metals are symbolized by a square (Au), pentagon (ITO), circle (Cu) and a diamond (Ag). From the color map, one can see that all four contact materials show a very similar behavior indicating that all four materials made a very similar type of contact to the Cu_2O .

The map of the J_{sc} shows low currents at the bottom and towards the right edge of the library, where the absorber thickness is low and where only a few photons are absorbed. At the top half towards the left part of the library higher current densities are measured, which unexpectedly seems to correlate with the total thickness ($\text{TiO}_2 + \text{Cu}_2\text{O}$) and less with the maximum Cu_2O absorber thickness. The V_{oc} on the other hand is rather constant, around 300 mV, throughout the library, while a fill factor of 40 – 45 % is achieved which drops towards 25% at the bottom of the library. The maximum power density, P_{max} , which is a product of the J_{sc} , V_{oc} , and fill factor, shows a similar behavior as the J_{sc} due to the low changes of V_{oc} and fill factor in this region.

Maps of the shunt and series resistance, R_{sh} and R_s , derived from I - V curves in the dark and under illumination are shown in Fig. 4. The series resistance drastically increases from $\sim 20 \Omega\text{cm}^2$ towards several $\text{k}\Omega\text{cm}^2$ at the bottom of the library where the Cu_2O is thin (Fig. 4a & c) for measurements in the dark and

under illumination. The resistance ratio R_s^{dark}/R_s^{light} indicates that R_s does not change significantly with illumination; only at the bottom of the library R_s is ~ 2.5 times larger in the dark than under illumination (Fig. 4e). A low R_s is desired for solar cell operation to minimize the R_s related losses of the fill factor.

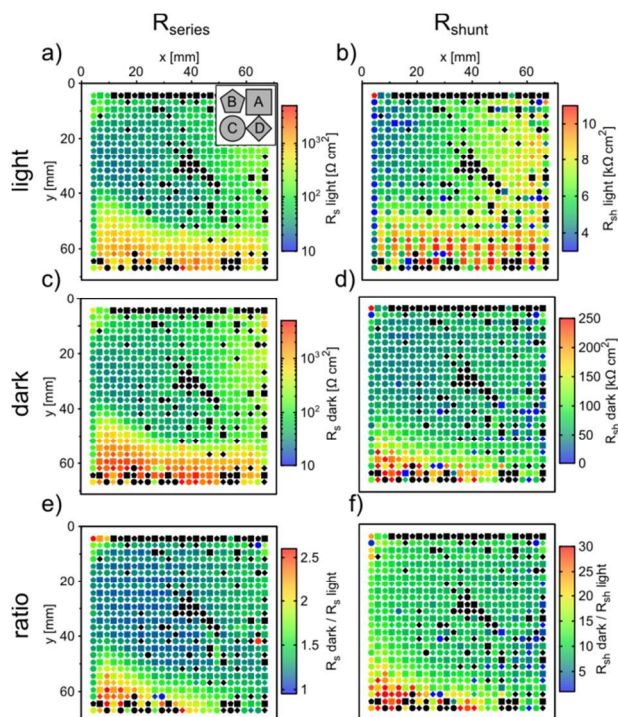


Figure 4. a) Series resistance, R_s , derived from I-V curves under illumination. b) Shunt resistance, R_{sh} , under illumination. c) R_s derived from dark I-V. d) R_{sh} in the dark. e) R_s dark divided by R_s light. f) R_{sh} dark divided by R_{sh} light.

The shunt resistance, R_{sh} , on the contrary should be large for good solar cell operation, and in the $\text{TiO}_2/\text{Cu}_2\text{O}$ hetero-junction library values between 3 – 11 $\text{k}\Omega\text{cm}^2$ were observed under illumination (Fig. 4b), and up to 250 $\text{k}\Omega\text{cm}^2$ in the dark (Fig. 4d). The R_{sh} in the dark is approximately 10 times larger at the top 2/3 of the library than R_{sh} under illumination (Fig. 4f), which is an undesired effect. Comparison with Fig. 2 indicates that the resistance is closely connected with the average crystal size, which is smallest at the bottom of the library. The impact of the crystallite size on the transport properties for Cu_2O has also been discussed by others and lead to the conclusion that large crystal grains are required for well performing solar cells.⁴⁵

The J_{sc} , V_{oc} , fill factor, and R_s under illumination as a function of the Cu_2O thickness are shown in Figure 5. From Fig. 5a one can see that the J_{sc} keeps increasing with the absorber thickness however with rather scattered points. The highest J_{sc} of this library is achieved at cells with lower Cu_2O thickness around 100 nm. These cells have the thickest TiO_2 (~ 500 nm), and are located toward the left edge of the library. The fact that the TiO_2 electron conducting layer thickness also has an impact on the J_{sc} is not fully understood. The origin for the TiO_2 thickness impact might be due to optical interference effects, generating a local maximum of the electric field above band gap light in the absorber for the mentioned specific combination of TiO_2 and Cu_2O thickness. We note that all the photocurrent densities of the library are significantly lower

when comparing to high performance $\text{ZnO}/\text{Cu}_2\text{O}$ hetero-junction cells. We attribute this to the significant lower Cu_2O crystal size which does not exceed ~ 150 nm. This leads to a high density of grain boundaries at which recombination takes place.

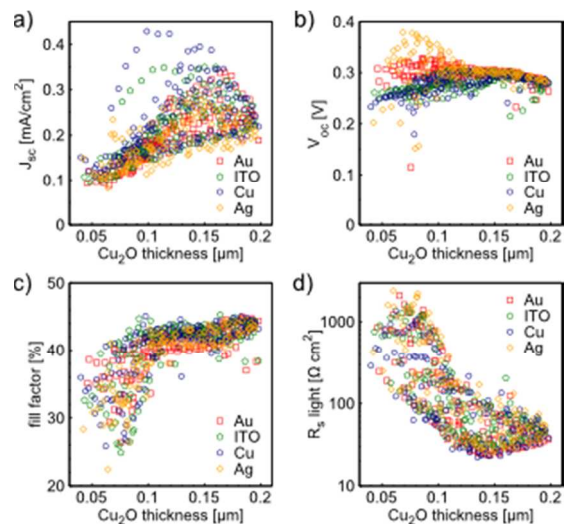


Figure 5. a) J_{sc} , b) V_{oc} , c) fill factor and d) R_s as a function of the Cu_2O absorber thickness.

It also should be noted that the most efficient Cu_2O PV cells today are based on thermal oxidation of highly pure Cu metal, which is a synthesis known to provide large Cu_2O crystals and subsequently a large diffusion length for efficient charge collection.^{14, 19, 45} The problem of a short diffusion length on the other hand is known from electrochemically deposited layers with smaller Cu_2O crystal size.^{12, 15}

Conversely, the V_{oc} remains very constant at 300 mV, and shows only a weak Cu_2O thickness dependence below 100 nm. Cells with a Ag contact show $V_{oc} > 300$ mV, cells with a Au contact show a constant V_{oc} throughout the entire thickness range, and ITO and Cu contacts show a $V_{oc} < 300$ mV, below 100 nm (Fig. 5b). A low V_{oc} has also been reported for $\text{TiO}_2/\text{Cu}_2\text{O}$ heterojunctions produced by electrophoretic deposition (TiO_2) and electro-deposition (Cu_2O), which did not exceed 250 mV.³⁰ The low photovoltage relative to the band gap of the Cu_2O is likely due to a large conduction band offset at the $\text{TiO}_2/\text{Cu}_2\text{O}$ interface, which can be in the order of 1 eV.⁴⁶

The fill factor is above 40% for cells with a Cu_2O layer thicker than 100 nm. Below 100 nm the fill factor is lower due to a high series resistance above 100 Ωcm^2 caused by the small Cu_2O crystal size. One can see that the performance of the solar cells is rather independent of the type of back contact material. Furthermore, the I-V curves do not show any indication for an energy barrier between the Cu_2O and the back contact which would lead to a non-ohmic behavior with an s-shaped I-V characteristic. This particularly interesting for the transparent ITO back contact in conjunction with the semi-transparent Cu_2O to design semi-transparent PV cells.

Conclusions

We have shown that the open circuit voltage of $\text{TiO}_2 / \text{Cu}_2\text{O}$ hetero-junctions is limited to approximately 300 mV and is nearly independent of the MO layer thickness or the type of back contact. We observe that Au, ITO, Cu, and Ag back

contacts show an ohmic behavior in the photocurrent range up to 0.5 mA/cm². These photocurrent densities in the sub mA/cm² regime are far below reported values for ZnO/Cu₂O or Ga₂O₃/Cu₂O hetero junction cells. This can be either due to poor charge separation at the TiO₂/Cu₂O interface or recombination within the Cu₂O due to the much smaller grain size of PLD synthesized Cu₂O compared to Cu₂O produced from thermally oxidized copper sheets. Furthermore, we observe a strong correlation between the size of the Cu₂O crystals and the shunt and series resistance, R_{sh} and R_s , respectively. At very low Cu₂O thicknesses a drop in the fill factor, down to 25%, is observed due to a strong increase of the series resistance, R_s , which can be attributed to the very small Cu₂O grain size <50 nm in that region of the library. The successful application of combinatorial material science to thin film photovoltaics opens a path for rapid screening of novel all-oxide photovoltaic systems.

Acknowledgements

This study was funded by the European Commission under the FP7 AllOxidePV project "Novel Composite Oxides by Combinatorial Material Synthesis for Next Generation All-Oxide-Photovoltaics" number 309018.

Notes and references

^a Department of Chemistry, Bar Ilan University, Ramat Gan 52900, Israel.

^b Department of Materials and Interfaces, Weizmann Institute of Science, Rehovot 76100, Israel.

* authors contributed equally.

1. A. Jäger-Waldau, *Int. J. Photoenergy*, 2012, **2012**, Article ID 768368.
2. G. Masson, M. Latour and D. Biancardi, *Global Market Outlook for Photovoltaics Until 2016*, European Photovoltaic Industry Association, 2012.
3. C. Wadia, A. P. Alivisatos and D. M. Kammen, *Environmental Science & Technology*, 2009, **43**, 2072-2077.
4. L. M. Peter, *J. Phys. Chem. Lett.*, 2011, **2**, 1861-1867.
5. H.-S. Kim, J.-W. Lee, N. Yantara, P. P. Boix, S. A. Kulkarni, S. Mhaisalkar, M. Grätzel and N.-G. Park, *Nano Lett.*, 2013, **13**, 2412-2417.
6. M. M. Lee, J. Teuscher, T. Miyasaka, T. N. Murakami and H. J. Snaith, *Science*, 2012.
7. J. H. Noh, N. J. Jeon, Y. C. Choi, M. K. Nazeeruddin, M. Grätzel and S. I. Seok, *Journal of Materials Chemistry A*, 2013, **1**, 11842-11847.
8. S. Rühle, M. Shalom and A. Zaban, *ChemPhysChem*, 2010, **11**, 2290-2304.
9. V. González-Pedro, X. Xu, I. Mora-Seró and J. Bisquert, *ACS Nano*, 2010, **4**, 5783-5790.
10. S. Greenwald, S. Rühle, M. Shalom, S. Yahav and A. Zaban, *PCCP*, 2011, **13**, 19302-19306.
11. T. Dittrich, A. Belaidi and A. Ennaoui, *Sol. Energy Mater. Sol. Cells*, 2011, **95**, 1527-1536.
12. K. P. Musselman, A. Marin, L. Schmidt-Mende and J. L. MacManus-Driscoll, *Adv. Funct. Mater.*, 2012, **22**, 2202-2208.
13. B. Kramm, A. Laufer, D. Reppin, A. Kronenberger, P. Hering, A. Polity and B. K. Meyer, *Appl. Phys. Lett.*, 2012, **100**, -.
14. T. Minami, Y. Nishi, T. Miyata and J.-i. Nomoto, *Applied Physics Express*, 2011, **4**, 062301.
15. B. D. Yuhas and P. Yang, *J. Am. Chem. Soc.*, 2009, **131**, 3756-3761.
16. S. Ishizuka, K. Suzuki, Y. Okamoto, M. Yanagita, T. Sakurai, K. Akimoto, N. Fujiwara, H. Kobayashi, K. Matsubara and S. Niki, *Physica status solidi (c)*, 2004, **1**, 1067-1070.
17. J. Katayama, K. Ito, M. Matsuoka and J. Tamaki, *J. Appl. Electrochem.*, 2004, **34**, 687-692.
18. B. K. Meyer, A. Polity, D. Reppin, M. Becker, P. Hering, P. J. Klar, T. Sander, C. Reindl, J. Benz, M. Eickhoff, C. Heiliger, M. Heinemann, J. Bläsing, A. Krost, S. Shokovets, C. Müller and C. Ronning, *phys. status solidi b*, 2012, **249**, 1487-1509.
19. T. Minami, Y. Nishi and T. Miyata, *Applied Physics Express*, 2013, **6**, 044101.
20. S. Rühle, A. Y. Anderson, H.-N. Barad, B. Kupfer, Y. Bouhadana, E. Rosh-Hodesh and A. Zaban, *J. Phys. Chem. Lett.*, 2012, **3**, 3755-3764.
21. J. Morasch, S. Li, J. Brötz, W. Jaegermann and A. Klein, *phys. status solidi a*, 2013, n/a-n/a.
22. D. S. Ginley and C. Bright, *MRS Bull.*, 2000, **25**, 15-18.
23. J. D. Perkins, J. A. del Cueto, J. L. Alleman, C. Warm Singh, B. M. Keyes, L. M. Gedvilas, P. A. Parilla, B. To, D. W. Readey and D. S. Ginley, *Thin Solid Films*, 2002, **411**, 152-160.
24. M. Reiser, K. Stöwe and W. F. Maier, *ACS Comb. Sci.*, 2012, **14**, 378-387.
25. A. I. Mardare, A. Savan, A. Ludwig, A. D. Wieck and A. W. Hassel, *Corros. Sci.*, 2009, **51**, 1519-1527.
26. M. S. Beal, B. E. Hayden, T. Le Gall, C. E. Lee, X. Lu, M. Mirsaneh, C. Mormiche, D. Pasero, D. C. A. Smith, A. Weld, C. Yada and S. Yokoishi, *ACS Comb. Sci.*, 2011, **13**, 375-381.
27. A. Stepanovich, K. Sliozberg, W. Schuhmann and A. Ludwig, *Int. J. Hydrogen Energy*, 2012, **37**, 11618-11624.
28. A. Teichler, R. Eckardt, S. Hoepfener, C. Friebe, J. Perelaer, A. Senes, M. Morana, C. J. Brabec and U. S. Schubert, *Adv. Energy Mater.*, 2011, **1**, 105-114.
29. R. Potyrailo, K. Rajan, K. Stoewe, I. Takeuchi, B. Chisholm and H. Lam, *ACS Comb. Sci.*, 2011, **13**, 579-633.
30. M. Ichimura and Y. Kato, *Mater. Sci. Semicond. Process.*, 2013, **16**, 1538-1541.
31. S. Rühle, S. Yahav, S. Greenwald and A. Zaban, *J. Phys. Chem. C*, 2012, **116**, 17473-17478.
32. B. O'Regan and D. T. Schwartz, *J. Appl. Phys.*, 1996, **80**, 4749-4754.
33. A. Y. Anderson, Y. Bouhadana, H.-N. Barad, B. Kupfer, E. Rosh-Hodesh, H. Aviv, Y. R. Tischler, S. Rühle and A. Zaban, *ACS Comb. Sci.*, 2014.
34. W. Thiess, Germany, 2012.
35. S. K. O'Leary, S. R. Johnson and P. K. Lim, *J. Appl. Phys.*, 1997, **82**, 3334.
36. C. Malerba, F. Biccari, C. Leonor Azanza Ricardo, M. D'Incau, P. Scardi and A. Mittiga, *Sol. Energy Mater. Sol. Cells*, 2011, **95**, 2848-2854.
37. S. Anisimov, D. Bäuerle and B. Luk'yanchuk, *Phys. Rev. B*, 1993, **48**, 12076-12081.
38. P. K. Schenck, N. D. Bassim, M. Otani, H. Oguchi and M. L. Green, *Appl. Surf. Sci.*, 2007, **254**, 781-784.
39. D. Bäuerle, *Appl. Phys. A - Mater.*, 1989, **48**, 527-541.
40. L. C. Olsen, R. C. Bohara and M. W. Urie, *Appl. Phys. Lett.*, 1979, **34**, 47-49.
41. L. Papadimitriou, N. A. Economou and D. Trivich, *Solar Cells*, 1981, **3**, 73-80.
42. J. Tauc, R. Grigorovici and A. Vancu, *phys. status solidi b*, 1966, **15**, 627-637.
43. P. E. de Jongh, D. Vanmaekelbergh and J. J. Kelly, *Chem. Mater.*, 1999, **11**, 3512-3517.
44. A. Cravino, P. Schilinsky and C. J. Brabec, *Adv. Funct. Mater.*, 2007, **17**, 3906-3910.
45. A. Mittiga, E. Salza, F. Sarto, M. Tucci and R. Vasanthi, *Appl. Phys. Lett.*, 2006, **88**, 163502-163502.
46. Y. Bessekhoud, D. Robert and J. V. Weber, *Catal. Today*, 2005, **101**, 315-321.